

# Can Tumor Cells be Distinguished from Blood Cells by Mechanical Parameters?

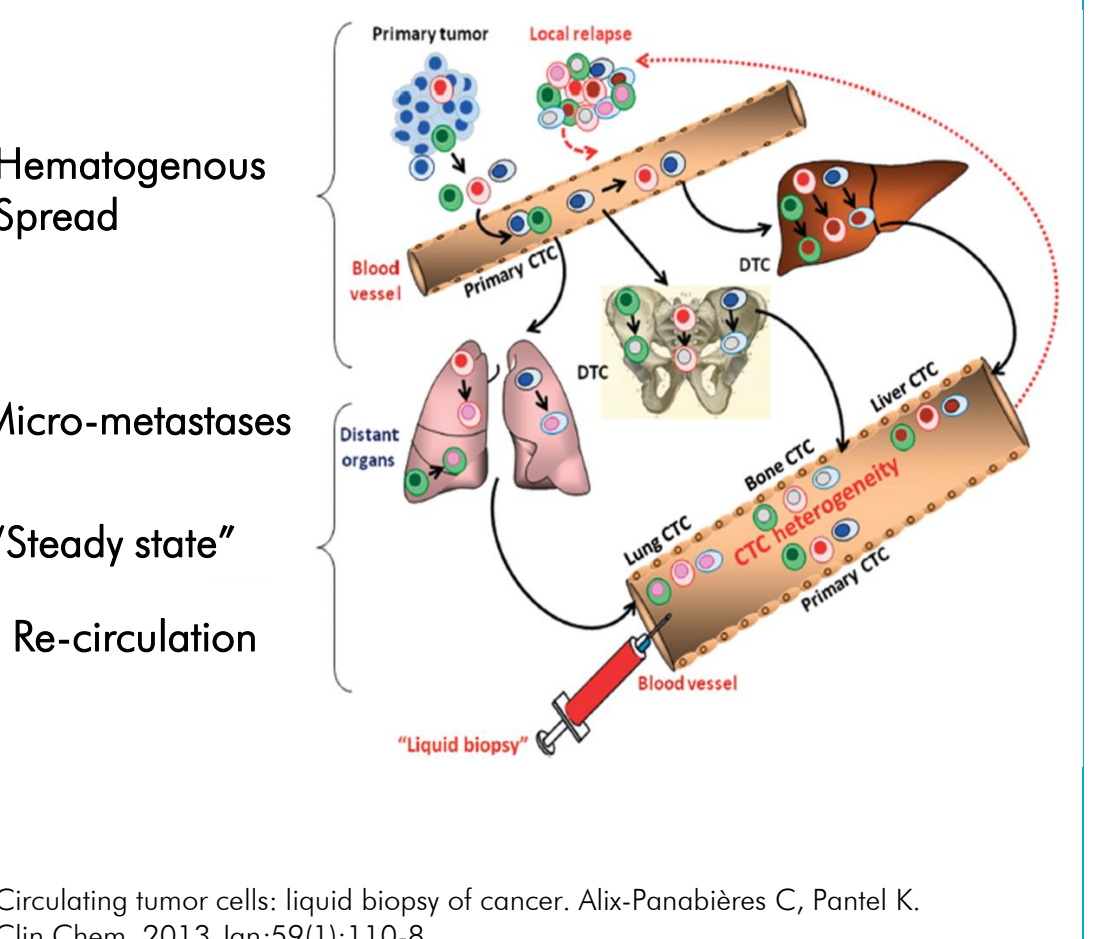
## A Label-Free CTC Detection Approach

Nel Ivonne<sup>1,\*†</sup>, Morawetz Erik W.<sup>2,\*</sup>, Dimitrij Tschodu<sup>2</sup>, Käs Josef A.<sup>2</sup> and Aktas Bahriye<sup>1</sup>

<sup>1</sup>University of Leipzig, Medical Center, Dept. of Gynecology  
<sup>2</sup>Soft Matter Physics Division, Peter-Debye-Institute Leipzig  
\*Both authors contributed equally to this paper  
† Correspondence: ivonne.nel@medizin.uni-leipzig.de

## BACKGROUND

Even years after successful treatment of the primary tumor about one third of the breast cancer patients are suffering from metastatic relapse. One reason might be hematogenous spread during early disease stages when isolated tumor cells disseminate from the primary tumor site. However, during their journey the tumor cells change their cellular properties and a variety of very heterogeneous CTC-subpopulations can be found in the peripheral blood. In contrast to conventional tumor tissue biopsies, CTCs could serve as "liquid biopsy". It is an advantage that blood samples can be obtained non-invasively and frequently during clinical routine. Thus, CTCs are a potential predictive surrogate marker for disease monitoring. But the low concentration of CTC in the peripheral blood as well as the sparse knowledge about their phenotype and its changes during cancer progression and treatment response makes it very difficult to separate them from hematopoietic cells. Here we focused on the viscoelastic passive and active contractile resistance of CTCs to evaluate the utility of mechanical parameters for CTC separation from blood.



Circulating tumor cells: liquid biopsy of cancer. Alix-Panabières C, Pantel K. Clin Chem. 2013 Jan;59(1):110-8

## RESULTS

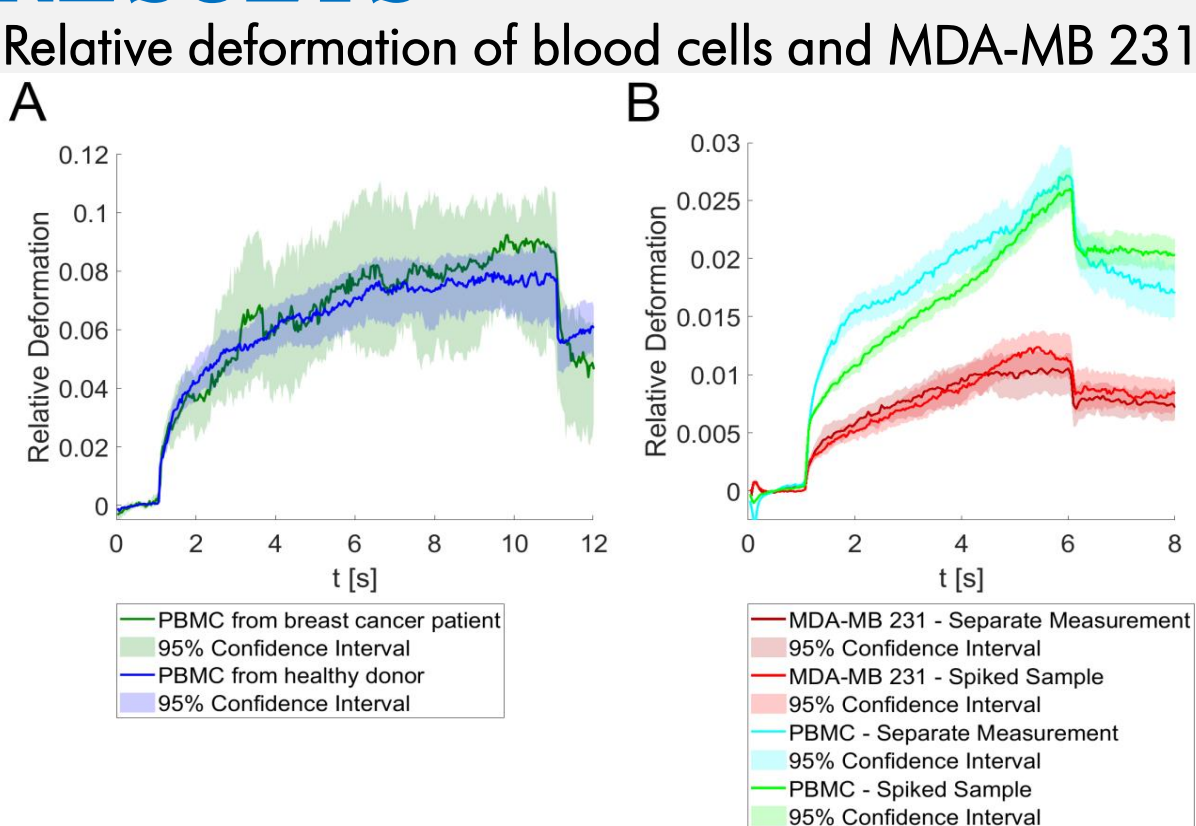


Figure 3. Relative deformation curves of blood cells and MDA-MB 231. A) PBMC from a healthy donor (blue line) and from a patient with breast cancer (green line) exhibited the same deformation behavior at 1200 mW stretching power. Relative deformations of the two samples were not distinguishable. B) We analyzed the relative deformation of PBMC samples ( $n=2098$  cells, light blue line, separate measurement). We then measured the relative deformation of breast cancer cells from the highly invasive breast cancer cell line MDA-MB 231 (brown line separate measurement). The deformation patterns of both cell types were significantly different ( $p < 0.001$ ) at 875 mW. Further, PBMC samples were mixed with GFP-expressing MDA-MB 231 cells to mimic a clinical blood sample containing CTCs. In total 957 single cell experiments of MDA-MB 231 and 1517 single cell experiments of PBMC were performed. The fluorescence signal of the transfected MDA-MB 231 cells served as a definite identifier between the two intermixed cell populations and was used as an internal control upfront data analysis. The relative deformation curves of MDA-MB 231 cells (red line, spiked sample) and PBMC (green line, spiked sample) were significantly different ( $p < 0.001$ ). In comparison to MDA-MB 231 cells, PBMC were much softer and showed a twofold elevated relative deformation (Median relative deformation MDA-MB 231 = 0.012, Median relative deformation PBMC = 0.0245).

### Relative and elliptic deformation curves of blood cells compared to non-hematopoietic CTC candidates

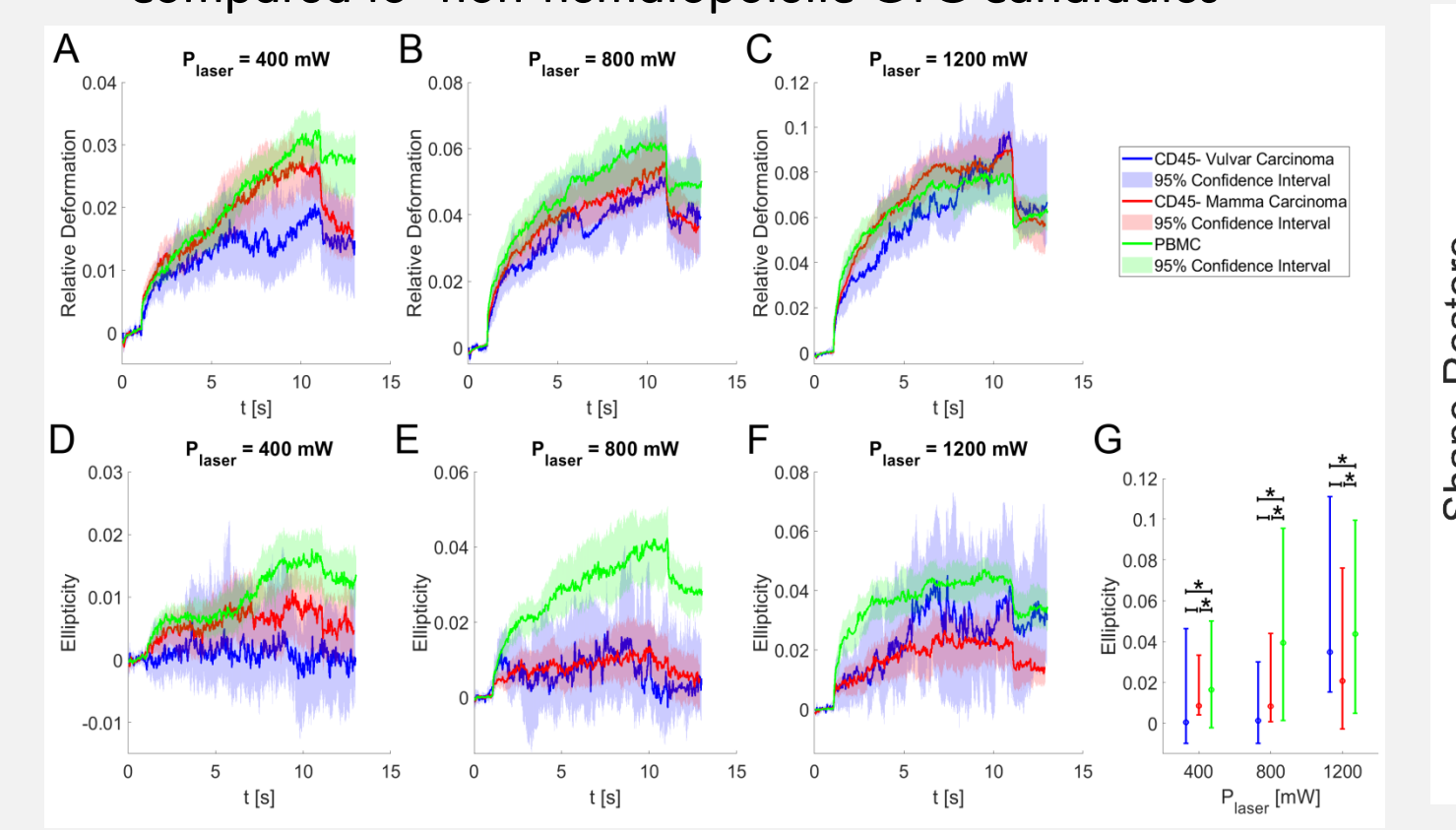


Figure 4. Relative and elliptic deformation curves of blood cells compared to non-hematopoietic CTC candidates from mamma and vulvar carcinoma patients. In total, we analyzed 1265 PBMC (green line) respective 1070 and 197 non-hematopoietic cells derived from 4 patients with breast cancer (red line) and one vulvar carcinoma patient (blue line). Measurements were carried out using three different laser powers  $P_1 = 400$  mW,  $P_2 = 800$  mW and  $P_3 = 1200$  mW, resulting in three different step stresses. A)-C) show the pooled relative deformation curves of possible CTC candidates from mamma and vulvar carcinoma compared to PBMC at each laser power. The deformation behavior of the three cell populations appeared to be similar, and only at  $P = 1200$  mW the relative deformation curves differed significantly at the end of the stretching phase ( $p = 0.001$ ). D)-F) show the elliptic deformation of all three cell populations at each laser power. The ellipticity of CTC candidates and PBMC differed significantly at each laser power indicating that in PBMC the elliptic deformation was increased by the factor 2 ( $p(P = 400$  mW) = 0.01,  $p(P = 800$  mW) < 0.001,  $p(P = 1200$  mW) < 0.001). G) Elliptic deformation of CTC candidates derived from patients with mamma and vulvar carcinoma was significantly lower at all laser powers compared to PBMC.

## METHODS

For proof of premise we used healthy peripheral blood mononuclear cells (PBMC) and human MDA-MB 231 breast cancer cells to create a CTC model system. For translational experiments CD45 negative cells were isolated from blood samples of patients with mamma or vulvar carcinoma. Cells were mechanically characterized in the optical stretcher (OS). Active and passive cell mechanical data were related with physiological descriptors by a random forest (RF) classifier to identify cell type specific properties.

Figure 1. Sample preparation and measurement: 1. Whole blood sample diluted with PBS; 2. Density gradient centrifugation; 3. Depletion of red blood cells using microbeads against glycoporphin  $\alpha$ ; 4. Resulting PBMC were resuspended and A) spiked with MDA-MB 231 breast cancer cells for proof of premise experiments to mimic CTC samples or B) incubated with microbeads against CD45 to deplete hematopoietic cells and thus enrich possible CTC candidates from clinical samples. Spiked respective remaining cell suspensions were applied to the optical stretcher and rheological parameters were measured.

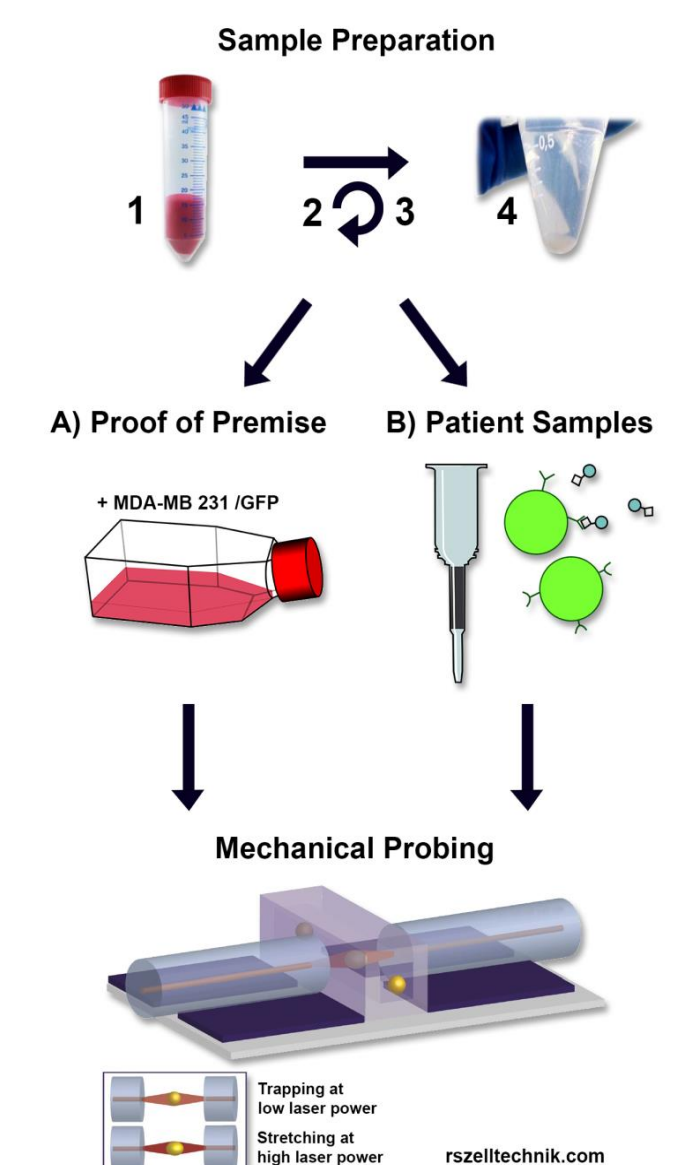


Table 1. Clinico-pathological characteristics. Patients were included after agreeing and signing a written informed consent.		
	Mamm carcinoma (n=5)*	Vulvar carcinoma (n=6)
Age (years)	31-78	62
Median	76	
Histology		
ductal	4	
lobular	1	
squamous epithelium	1	
Stage		
T1	4	
T2	1	
Lymphnode		
N0	3	
N1	1	
Nx	1	
Grade		
G1	1	
G2	2	
G3	2	1
Subtype		
luminal A	2	
luminal B	2	
triple negative	1	
Setting		
primary	4	
recurrent	1	
Therapy		
NACT	1	
adjuvant endocrine	4	-

\*Per proof of premise experiments we analysed PBMC obtained from a healthy donor (data not shown) compared to a breast cancer patient. For translational experiments we used blood samples from patients with mamma (n=4) and vulvar carcinoma (n=1). Therefore the experimental design results in the total number of 5 patients with mamma carcinoma (n=5).

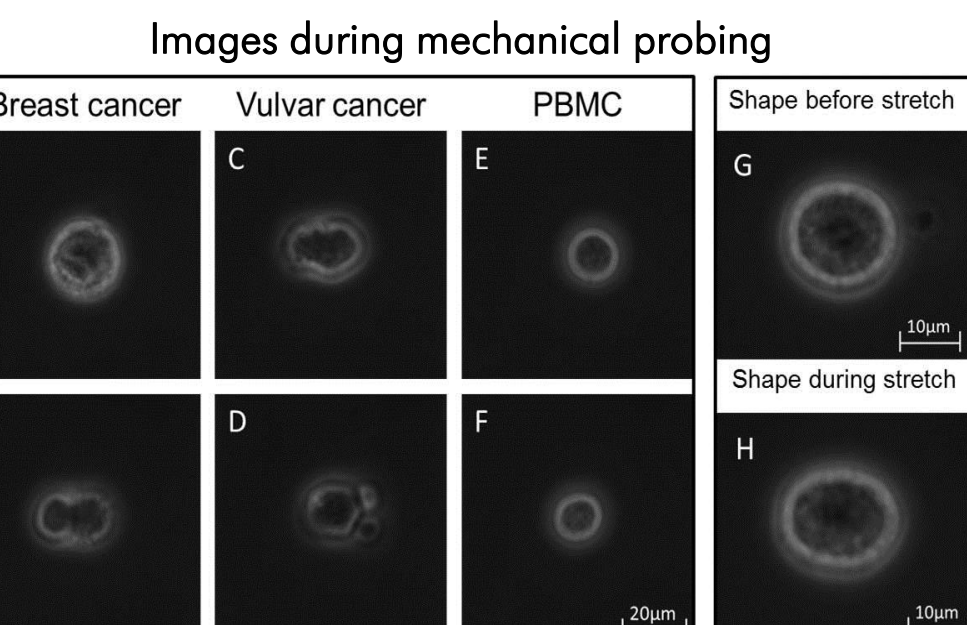


Figure 2. Representative phase contrast images obtained during mechanical probing using the optical stretcher. A) Possible CTC candidate and B) Cell Cluster – both detected in the CD45 depleted cell suspension from a breast cancer patient. C) Possible CTC candidate and D) Cell Cluster – from vulvar cancer patient. E) and F) show PBMC. G) and H) shape of a breast cancer derived CTC with particularly low mechanical resistance before and during stretching demonstrating that mechanical changes are very small.

### Shape Restoration of cells in the optical stretcher

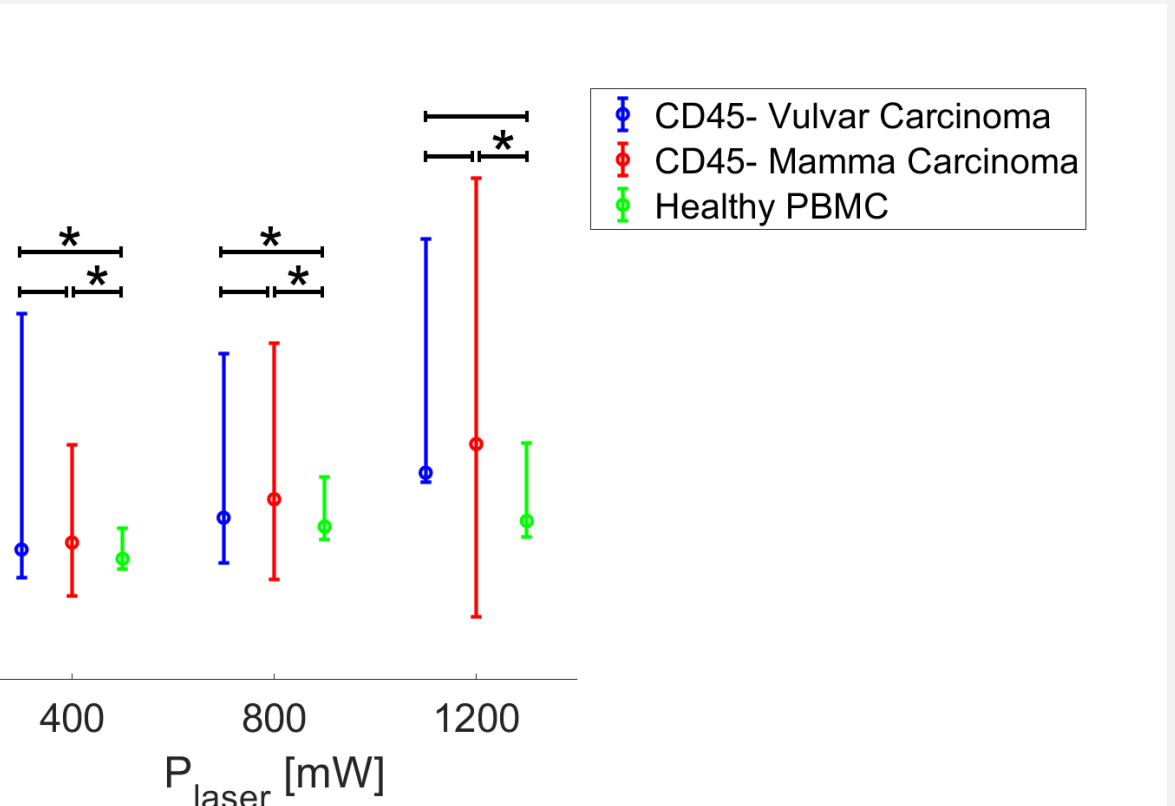


Figure 5. Shape Restoration of cells in the optical stretcher. After being exposed to the laser-induced step stress, cells were tending to restore their original shape. An adequate shape restoration parameter was the difference between the elongation at the end of the step stress and the elongation at 1.5 s after the step stress. At all laser powers, PBMC showed significantly lower shape restoration compared to CTC candidates from mamma carcinoma ( $p < 0.001$ ). Compared to CTCs from vulvar carcinoma, PBMC shape restoration was significantly lower only at 400 and 800 mW ( $p < 0.05$ ), but not at 1200 mW. Shape restoration of CTC candidates from mamma and vulvar carcinomas was similar.

### Shape restore increased prediction performance

Table 2. Prediction using random forest algorithm

	excluding shape restoration			including shape restoration			
Laser Power [mW]	Accuracy	Sensitivity	Specificity	Laser Power [mW]	Accuracy	Sensitivity	Specificity
400	0.73	0.73	0.73	400	0.72	0.71	0.71
800	0.74	0.73	0.73	800	0.74	0.73	0.73
1200	0.75	0.74	0.74	1200	0.74	0.73	0.73
average	0.74	0.73	0.73	average	0.73	0.72	0.72
pooled	0.71	0.69	0.69	pooled	0.74	0.73	0.73

Table 2. Prediction performance of the random forest machine learning algorithm applied to our optical stretcher data set of 1070 non-hematopoietic cells from breast cancer patients and 1265 PBMC. Cells were tested in step stress experiments at various laser powers, and physiological parameters as well as cellular deformation were recorded. Kelvin Voigt modeling was applied to the data to derive a number of active and passive rheological parameters. The prediction power slightly increased from 400 mW over 800 mW to 1200 mW. When data from all three laser powers were pooled before applying the RF algorithm, accuracy was 0.71, sensitivity and specificity were 0.69, respectively. Interestingly, when shape restoration/relaxation was included accuracy, sensitivity and specificity increased to 0.74 and 0.73, respectively.

## SUMMARY & CONCLUSIONS

- MDA-MB 231 cells could be clearly distinguished from PBMC based on their mechanical parameters obtained from OS measurements
- Analysis of clinical samples revealed that in PBMC the elliptic deformation was significantly increased compared to CTCs.
- CTCs showed significantly higher shape restoration compared to PBMC.
- Based on Kelvin-Voigt modeling, the RF algorithm revealed that the OS discriminated CTCs from PBMC with an accuracy of 0.74, a sensitivity and specificity of 0.73, respectively.
- CTCs exhibit mechanical features that favor their escape from the vascular system. Together with cell morphology the mechanical deformation pattern might be an appropriate tool for marker-free CTC detection.

### Impact of morphological and mechanical effects

Table 3. Progressive input data matrix			
Stepwise data input	Accuracy	Sensitivity	Specificity
1 Cell area, cell radius	0.54	0.53	0.53
2 Relative deformation	0.66	0.64	0.64
3 Elliptic deformation	0.69	0.69	0.68
4 Shape restoration	0.71	0.71	0.7

Table 3. Progressive input data matrix. To distinguish morphological from mechanical effects, we constructed an input data matrix starting with the morphological parameters cell area and cell radius only, and then progressively added the mechanical features relative deformation, elliptical deformation, and shape restoration. The prediction results were computed for the laser power of 1200 mW and revealed superior accuracy, sensitivity and specificity when mechanical parameters were included.